JOURNAL OF MAGNETIC RESONANCE **124,** 372–382 (1997)
ARTICLE NO. MN961041

A Robust Method for Estimating Cross-Relaxation Rates from Simultaneous Fits to Build-Up and Decay Curves*

IGOR NAJFELD, KWAKU T. DAYIE, GERHARD WAGNER, AND TIMOTHY F. HAVEL

Biological Chemistry and Molecular Pharmacology, Harvard Medical School, 240 Longwood Avenue, Boston, Massachusetts 02115

Received July 17, 1996; revised October 17, 1996

This paper introduces a novel computational method for estimating relaxation rates among pairs of spin orders. This method simultaneously estimates all the auto- and cross-relaxation rates from the same measurements, and avoids the ill-conditioning problems associated with multiexponential fits. The method models the relaxation dynamics by a system of linear differential equations, and assumes that measurements of the spin orders have been made at an equally spaced sequence of time points. It computes a nonlinear least-squares fit of the exponential of the rate matrix at the shortest time point to these measurements. Preliminary estimates of the exponential matrix and initial spin orders from which to start the computations are obtained by solving simpler linear-least-squares problems. The performance of the method on simulated 2 × 2 test problems indicates that when measurements at eight or more equally spaced times spanning the maximum and inflection points of the build-up curves are available, the relative errors in the rates are usually less than the relative errors in the measurements. The method is further demonstrated by applying it to the problem of determining the cross correlation-induced cross-relaxation rates between the in-phase and antiphase coherence of the amide groups in the ^{15}N-labeled protein oxidized flavodoxin. Finally, the possibility of extending the method to other kinds of relaxation measurements and larger spin systems is discussed.

INTRODUCTION

Relaxation rates contain important information on molecular conformation and dynamics (*1*). In our laboratory, considerable attention has been given to the determination of the auto- and cross-relaxation rates among the various spin orders in the amide groups of proteins, since these enable one to ''map'' their spectral-density functions directly (*2*). While well-established methods of determining the auto-relaxation rates are available, the determination of the (usually much smaller) cross-relaxation rates is often experimentally and computationally challenging. Cross relaxation induced by cross correlation between the dipole–dipole interaction and chemical-shift anisotropy in the amide groups of proteins is a case of particular interest, since the corresponding cross-relaxation rates can potentially yield additional data for use in spectral-density mapping, but these effects have proven difficult to measure accurately in macromolecules (*3–7*).

The most common procedure for estimating cross-relaxation rates starts by suppressing the coherence-transfer pathways responsible for the cross relaxation, in order to determine the auto-relaxation rates from monoexponential fits. Then the eigenvalues of the relaxation matrix are estimated from multiexponential fits without suppression of the cross relaxation and used, together with the auto-relaxation rates, to derive the cross-relaxation rates. Unfortunately, direct fits to multiple decaying exponentials is a notoriously *ill-conditioned* problem (*8*). This means that the noise and other errors present in the integrated cross-peak intensities produce even larger errors in the estimated relaxation rates, because the intensities do not change significantly over large but compensating changes in the rates. This difficulty, it should be noted, is entirely distinct from the multiple-minimum problem, and often occurs even in *linear*-least-squares problems (*9*). An example that arises in the interpretation of NMR data may be found in Ref. (*10*).

In this paper, we describe a simpler and more direct method for estimating cross-relaxation rates that both avoids the need to determine the auto-relaxation rates independently and at the same time avoids the problems associated with multiexponential fits. This approach is developed and evaluated in the special case of a 2 × 2 symmetric relaxation matrix, but it should be possible to extend it to larger spin systems. The main idea is to directly estimate the exponential of the relaxation matrix by fitting the build-up and decay measurements at a sequence of time points. Providing that these time points are equally spaced, the properties of the matrix exponential and its derivatives (*11*) enable us to solve this *inverse problem* using standard linear- and nonlinear-

* Preliminary accounts of this work were presented at the 36th Experimental Nuclear Magnetic Resonance Conference, March 1995, Boston, Massachusetts, and the 50th International Society for Magnetic Resonance Conference, July 1995, Sydney, Australia.

1090-7807/97 $25.00

least-squares procedures. In the case of a 2×2 matrix exponential, we have also derived an analytic formula for the relaxation rates.

Our results with simulated data indicate that, providing measurements at eight or more well-placed time points are available, the relative errors in the estimated rates are usually less than the relative errors in the individual measurements. The method is further illustrated by an application to the determination of the rate of conversion of antiphase to in-phase coherence in the amide groups of the ^{15}N-labeled protein, oxidized flavodoxin, which is due to chemical-shift anisotropy/dipole–dipole cross correlation. Finally, the potential of the method as a general means of estimating relaxation matrices is discussed.

THEORY

The relaxation among a pair of spin orders that are isolated from all other spin orders in the molecule is governed by a 2×2 symmetric system of ordinary linear differential equations with constant coefficients (*2*), i.e.,

$$\frac{d\mathbf{q}}{dt} \equiv \begin{bmatrix} da/dt \\ db/dt \end{bmatrix} = \begin{bmatrix} \rho_a & \sigma \\ \sigma & \rho_b \end{bmatrix} \cdot \begin{bmatrix} a(t) \\ b(t) \end{bmatrix} \equiv \mathbf{R} \cdot \mathbf{q}. \quad [1]$$

We have labeled the two components of the spin-order vector $\mathbf{q} = \mathbf{q}(t)$ as ''*a*'' and ''*b*'', and adsorbed the usual minus signs into the rates. Thus the rates ρ_a and ρ_b are negative, and the condition $\sigma^2 < \rho_a\rho_b$ implies that the relaxation matrix $\mathbf{R}$ itself is *stable* (i.e., that its eigenvalues are negative). In the following, we shall refer to ρ_a and ρ_b as the *auto-relaxation* and σ as the *cross-relaxation* rates. Equation [1], of course, is applicable to many different relaxation processes, regardless of the mechanism of relaxation.

The formal solution to Eq. [1] is given by

$$\mathbf{q}(t) = \exp(t\mathbf{R}) \cdot \mathbf{q}(0), \quad [2]$$

where the exponential of the matrix $t\mathbf{R}$ may be defined by its Taylor series $\exp(t\mathbf{R}) = \mathbf{I} + t\mathbf{R} + (t\mathbf{R})^2/2! + \cdots$ and $\mathbf{q}(0)$ is the initial spin-order vector. Since the powers of a symmetric matrix are symmetric, $\exp(t\mathbf{R})$ inherits the symmetry of $\mathbf{R}$. In order to obtain the 2×2 matrix exponential in closed form, we define

$$\mathbf{S} \equiv \mathbf{R} - \alpha\mathbf{I} = \begin{bmatrix} \delta & \sigma \\ \sigma & -\delta \end{bmatrix}, \quad [3]$$

where $\alpha \equiv \mathrm{tr}(\mathbf{R})/2$ is half the trace and $\delta \equiv (\rho_a - \rho_b)/2$. Since the identity matrix $\mathbf{I}$ commutes with any matrix, the exponential factorizes as $\exp(t\mathbf{R}) = \exp(t\alpha)\exp(t\mathbf{S})$. Moreover, the characteristic equation for $\mathbf{S}$ is $\mathbf{S}^2 = \beta^2\mathbf{I}$, where

$$\beta^2 \equiv \delta^2 + \sigma^2 = -\det(\mathbf{S}). \quad [4]$$

Collecting even and odd terms in the Taylor series for $\exp(t\mathbf{S})$ thus yields an analytic formula for the exponential of the relaxation matrix

$$\begin{aligned} \exp(t\mathbf{R}) &= e^{t\alpha}e^{t\mathbf{S}} \\ &= e^{t\alpha}(\mathbf{I}\cosh(t\beta) + \mathbf{S}\sinh(t\beta)/\beta) \\ &= e^{t\alpha}\begin{bmatrix} \cosh(t\beta) + \delta\sinh(t\beta)/\beta & \sigma\sinh(t\beta)/\beta \\ \sigma\sinh(t\beta)/\beta & \cosh(t\beta) - \delta\sinh(t\beta)/\beta \end{bmatrix}. \end{aligned} \quad [5]$$

In the following, we shall denote the functions of time obtained by suppressing the dependence of the exponential on the relaxation matrix $\mathbf{R}$ by $\mathbf{F}(t) \equiv [f_{ij}(t)] \equiv \exp(t\mathbf{R})$.

The relaxation matrix $\mathbf{R}$ can be obtained from the matrix exponential $\mathbf{F} \equiv [f_{ij}]$ at a fixed point t in time as follows. First, we use Eq. [5] to evaluate the two ratios

$$\xi = \frac{f_{11} - f_{22}}{2f_{12}} = \frac{\delta}{\sigma} \quad [6]$$

and

$$\eta = \frac{2f_{12}}{f_{11} + f_{22}} = \frac{\sigma}{\beta}\tanh(t\beta) = \frac{\tanh(t\sigma\sqrt{1+\xi^2})}{\sqrt{1+\xi^2}}. \quad [7]$$

On inverting Eq. [7] and rearranging, we obtain the cross-relaxation rate as

$$\sigma = \frac{\mathrm{arctanh}(\eta\sqrt{1+\xi^2})}{t\sqrt{1+\xi^2}}. \quad [8]$$

Next, we use Eq. [6] to compute $\delta = \xi\sigma$, and then obtain α from the Jacobi identity (*12*), i.e.,

$$\alpha = \frac{\mathrm{tr}(\mathbf{R})}{2} = \frac{\log[\det(\mathbf{F})]}{2t}. \qquad [9]$$

Finally, the auto-relaxation rates are obtained from

$$\rho_a = \alpha + \delta \quad \text{and} \quad \rho_b = \alpha - \delta. \qquad [10]$$

This ''eigen-free'' approach avoids computing the matrix logarithm; it does, however, contain two scalar logarithms, one in Eq. [9] and the other hidden in the arctanh of Eq. [8]. Thus, these formulae will be numerically unstable only if $\det(\mathbf{F}) < \epsilon$ or $|\eta\sqrt{1+\xi^2}| > 1 - \epsilon$ for some $\epsilon > 0$ of order of the machine precision.

We now state some of the most important properties of the solution to Eq. [1], which have proved useful in the design and qualitative analysis of the experiments. Proofs may be obtained from the analysis of Eqs. [4] and [5]:

1. The auto-relaxation functions $f_{11}(t)$ and $f_{22}(t)$ are positive, bounded by one, convex, and strictly decreasing with time.
2. The cross-relaxation function $f_{12}(t)$ satisfies $\sigma f_{12}(t) \geqslant 0$ as well as $|f_{12}(t)| \leqslant f_{11}(t)$ if $\delta \geqslant 0$, or $|f_{12}(t)| \leqslant f_{22}(t)$ if $\delta \leqslant 0$.
3. The cross-relaxation function has a unique extremum at time $\tau_{\mathrm{ext}} = \mathrm{arctanh}(-\beta/\alpha)/\beta$, and a unique inflection point at $2\tau_{\mathrm{ext}}$.
4. At this extremum, we have $f_{11}(\tau_{\mathrm{ext}})/f_{22}(\tau_{\mathrm{ext}}) = \rho_a/\rho_b$ as well as $f_{12}(\tau_{\mathrm{ext}}) \leqslant \sigma/2$.

We now outline our procedure for estimating the relaxation matrix, which uses measurements of the spin-order vector $\mathbf{q}(t)$ at a sequence of *equally spaced* time points, and assumes that the relaxation rates are *independent* variables. The procedure itself consists of the following three steps. In the first step, a preliminary estimate of the initial spin order (if it cannot be measured directly), together with the exponential at the *shortest* time point, is obtained from two different linear-least-squares fits. In the second step, these preliminary estimates are used as the starting values for a nonlinear-least-squares fit, which more accurately models the relaxation dynamics including the initial condition; because such nonlinear fits are prone to being trapped in local minima, the preliminary estimates are nevertheless essential if a good fit is to be found reliably. In the final step, the relaxation matrix is calculated from the estimated exponential, using the inversion procedure given in Eqs. [6] through [10] above.

LINEAR ESTIMATES

Consider first the problem of estimating the initial spin-order vector $\mathbf{q}(0)$. Let $t_1, \ldots, t_M$ be the time points at which the inexact measurements $\mathbf{q}_m$ of the exact solution $\mathbf{q}(t_m)$ are taken, where $t_m = h \cdot m$ for some fixed $h > 0$ and $m = 1, \ldots, M$. We shall use the fact that the exponential of a symmetric matrix is symmetric, together with the well-known *addition formula*, $\exp(s\mathbf{R}) \cdot \exp(t\mathbf{R}) = \exp[(s+t)\mathbf{R}]$, to derive a new relation between the initial spin-order vector and the spin-order vectors at three time points t_m, t_n, and $t_{m+n} = t_m + t_n$ with $1 \leqslant m, n \leqslant m + n \leqslant M$, namely

$$\mathbf{q}(0)^{\mathrm{T}} \cdot \mathbf{q}(t_{m+n}) = \mathbf{q}(t_m)^{\mathrm{T}} \cdot \mathbf{q}(t_n). \qquad [11]$$

The proof goes as follows:

$$\begin{aligned} \mathbf{q}(t_m)^{\mathrm{T}} \cdot \mathbf{q}(t_n) &= [\exp(t_m\mathbf{R}) \cdot \mathbf{q}(0)]^{\mathrm{T}} \cdot [\exp(t_n\mathbf{R}) \cdot \mathbf{q}(0)] \\ &= \mathbf{q}(0)^{\mathrm{T}} \cdot \exp(t_m\mathbf{R}) \cdot \exp(t_n\mathbf{R}) \cdot \mathbf{q}(0) \\ &= \mathbf{q}(0)^{\mathrm{T}} \cdot \exp[(t_m + t_n)\mathbf{R}] \cdot \mathbf{q}(0) \\ &= \mathbf{q}(0)^{\mathrm{T}} \cdot \mathbf{q}(t_{m+n}). \end{aligned} \qquad [12]$$

If one component of the initial spin-order vector $\mathbf{q}(0) = [a(0), b(0)]^{\mathrm{T}}$ is known to be zero, e.g., $a(0) = 0$, this relation is sufficient to determine the other component $b(0) = [a(t_m)a(t_n) + b(t_m)b(t_n)]/b(t_{m+n})$. We mention that formula [11] is valid for an arbitrary sequence of time points $t_1, \ldots, t_M$ as long as each t_k is of the form $t_k = t_m + t_n$ with $1 \leqslant m, n < k \leqslant M$. Hence any arithmetic, geometric, or even Fibonacci sequence can be used.

Formula [11] gives us a means of estimating the initial condition of a solution to a symmetric system of linear differential equations. Thus, given approximate measurements $\mathbf{q}_1, \ldots, \mathbf{q}_M$ of the spin-order vectors $\mathbf{q}(t_1), \ldots, \mathbf{q}(t_M)$, we seek an estimate $\hat{\mathbf{q}}_0$ of the initial condition $\mathbf{q}(0)$ by satisfying *all* instances of Eq. [11] as closely as possible, in the least-squares sense. This leads to the following two-variable linear-least-squares problem in the unknown initial spin order $\mathbf{u}$:

$$\begin{aligned} \Phi(\hat{\mathbf{q}}_0) &= \min_{\mathbf{u}} [\Phi(\mathbf{u})] \\ &= \min_{\mathbf{u}} \Big(\sum_{m=1}^{\lfloor M/2 \rfloor} \sum_{n=m}^{M-m} \|\mathbf{q}_{m+n}^{\mathrm{T}} \cdot \mathbf{u} - \mathbf{q}_m^{\mathrm{T}} \cdot \mathbf{q}_n\|^2 \Big). \end{aligned} \qquad [13]$$

On setting the gradient of Φ to zero, we obtain the normal equations for this problem, namely $\mathbf{A} \cdot \mathbf{u} = \mathbf{b}$, where

$$\mathbf{A} = \sum_{m=1}^{\lfloor M/2 \rfloor} \sum_{n=m}^{M-m} \begin{bmatrix} a_{m+n}^2 & a_{m+n}b_{m+n} \\ a_{m+n}b_{m+n} & b_{m+n}^2 \end{bmatrix}$$

$$\mathbf{b} = \sum_{m=1}^{\lfloor M/2 \rfloor} \sum_{n=m}^{M-m} \begin{bmatrix} (a_m a_n + b_m b_n) a_{m+n} \\ (a_m a_n + b_m b_n) b_{m+n} \end{bmatrix}. \qquad [14]$$

In the event that one component of the initial spin order is known to be zero, this becomes a univariate linear-least-squares problem whose solution is obtained from a single row of the equation $\mathbf{A}\cdot\mathbf{u}=\mathbf{b}$.

We now turn to the problem of obtaining a preliminary estimate $\hat{\mathbf{F}}_h$ of the matrix exponential at time h. Since

$$\mathbf{q}(t_{m+1})=\mathbf{F}(h)\cdot\mathbf{q}(t_m)\quad(1\leqslant m\leqslant M-1)\qquad[15]$$

by Eq. [2], it makes sense to try to satisfy these relations as closely as possible, once again in the least-squares sense. This leads to another linear-least-squares problem, namely

$$\begin{aligned}\Psi(\hat{\mathbf{F}}_h)&=\min_{\mathbf{V}}\,[\Psi(\mathbf{V})]\\&=\min_{\mathbf{V}}\,\Big(\sum_{m=1}^{M-1}\|\mathbf{V}\cdot\mathbf{q}_m-\mathbf{q}_{m+1}\|^2\Big),\end{aligned}\qquad[16]$$

where the minimum is now taken over all 2×2 symmetric matrices $\mathbf{V}$.

The normal equations for this problem are obtained by setting the gradient of Ψ with respect to the three *independent* elements of $\mathbf{V}=[v_{ij}]$ to zero. Letting $\mathbf{v}=[v_{11},\,v_{12},\,v_{22}]^{\mathrm{T}}$, these equations are written in matrix form as $\mathbf{C}\cdot\mathbf{v}=\mathbf{d}$, where

$$\mathbf{C}=\sum_{m=1}^{M-1}\begin{bmatrix}a_m^2 & a_mb_m & 0\\ a_mb_m & a_m^2+b_m^2 & a_mb_m\\ 0 & a_mb_m & b_m^2\end{bmatrix}$$

$$\mathbf{d}=\sum_{m=1}^{M-1}\begin{bmatrix}a_ma_{m+1}\\ a_mb_{m+1}+a_{m+1}b_m\\ b_mb_{m+1}\end{bmatrix}.\qquad[17]$$

Using the Cauchy–Schwarz inequality, it is easy to show that the determinant of this matrix vanishes only if $a_m=\varsigma b_m$ for some constant ς and all $1\leqslant m\leqslant M-1$. Hence the 3×3 matrix $\mathbf{C}$ (as well as the 2×2 matrix $\mathbf{A}$ in Eq. [14]) is well conditioned unless the initial spin-order vector $\mathbf{q}(0)$ is near the nonnegative eigenvector $\mathbf{r}$ of $\mathbf{R}$. Since $\mathbf{F}(t)=\exp(t\mathbf{R})$ has the *same* eigenvectors as $\mathbf{R}$, this means that $\mathbf{F}(t)\cdot\mathbf{q}(0)\approx\kappa(t)\mathbf{r}$ for some scalar function κ and all $t\geqslant 0$, so that the measurements $\mathbf{q}_m$ are nearly linearly dependent. Fortunately, in most experiments, we have $a(0)=0$ or $b(0)=0$, so this can happen only if the cross-relaxation rate σ is small compared to $\sqrt{\rho_a\rho_b}$ (in which case the build-up curve will probably be below the noise level). This can be ascertained from the data by means of Properties 3 and 4 in the previous section.

It may be observed that if a sequence of time points is given by $t_m=t_0+mh$, for some t_0, $h>0$ and integer $1\leqslant m\leqslant M$, then shifting all the times by t_0 affects only the initial condition, but *not* the derived rate matrix. Therefore, all of the above formulae for the matrix $\hat{\mathbf{F}}_h$ (as in Eq. [16]) may be used unchanged. More generally, it is not difficult to extend these formulae to the case in which the time points are distributed as $k_1h,\,k_2h,\,\ldots,\,k_mh$ for an arbitrary increasing sequence of integers $k_1<k_2<\cdots<k_m$.

NONLINEAR ESTIMATES

Once these preliminary estimates of the initial spin-order vector $\hat{\mathbf{q}}_0$ and the matrix $\hat{\mathbf{F}}_h$ have been obtained, they should be refined by means of the nonlinear-least-squares fit

$$\begin{aligned}\Omega(\mathbf{q}_0,\mathbf{F}_h)&=\min_{\mathbf{u},\mathbf{V}}\,[\Omega(\mathbf{u},\mathbf{V})]\\&=\min_{\mathbf{u},\mathbf{V}}\,\Big(\sum_{m=1}^{M}\|\mathbf{V}^m\cdot\mathbf{u}-\mathbf{q}_m\|^2\Big)\end{aligned}\qquad[18]$$

to obtain the final estimates $\mathbf{q}_0$, $\mathbf{F}_h$.

The least-squares fit in Eq. [18] tends to produce better results than that in Eq. [16] because it treats the initial condition as an unknown, and computes the entire time sequence from it together with the current estimate of the exponential matrix. Equation [16], in contrast, predicts the measurements at each time point from those at the preceding time point only, and is therefore more strongly affected by ''outliers.'' Although the function Ω in Eq. [18] may have numerous local minima, the preliminary estimates obtained from the previous step are already fairly good as a rule, and hence convergence to a satisfactory solution is almost always obtained. We should also point out that this least-squares fit is quite different from Prony's method, a classical method that has been used to interpolate and fit data points by a linear combination of scalar exponentials.

In this work, we have usually used a BFGS quasi-Newton method with a cubic line search to get close to a minimum of Ω, followed by a few iterations of Newton's method to attain machine precision. In some of our simulated test problems using small amounts of data containing very large errors, this procedure failed to converge. In such cases convergence can be obtained by varying the preliminary values of the initial spin orders and rates within a small range about the values as calculated above. Since divergence was seldom encountered with the experimental data (see below), we omit the details of this procedure.

Like most reasonably efficient nonlinear optimization methods, this procedure requires the first and second derivatives of the function Ω with respect to the variables $\mathbf{u}$, $\mathbf{V}$. If we let $\mathbf{z}_m=\mathbf{V}^m\cdot\mathbf{u}-\mathbf{q}_m$, the gradient can be written as $\nabla\Omega=2\,\Sigma_{m=1}^{M}\,(\nabla\mathbf{z}_m)^{\mathrm{T}}\cdot(\mathbf{z}_m-\mathbf{q}_m)$, where $\nabla\mathbf{z}_m$ denotes the 5×2 Jacobian matrix of the vector-valued function $\mathbf{z}_m=\mathbf{z}_m(\mathbf{u},\mathbf{V})$. The partials with respect to the initial spin-order

variables $\mathbf{u}$ can be expressed either as a recurrence relation or in closed form:

$$\frac{\partial \mathbf{z}_m}{\partial \mathbf{u}} = \mathbf{V} \cdot \frac{\partial \mathbf{z}_{m-1}}{\partial \mathbf{u}} = \cdots = \mathbf{V}^m \cdot \frac{\partial \mathbf{u}}{\partial \mathbf{u}} = \mathbf{V}^m. \quad [19]$$

A recurrence relation for the partials with respect to the variables v_{ij} is also straightforward, namely

$$\frac{\partial \mathbf{z}_m}{\partial v_{ij}} = \mathbf{V} \cdot \frac{\partial \mathbf{z}_{m-1}}{\partial v_{ij}} + \mathbf{E}_{ij} \cdot \mathbf{z}_{m-1} \quad (1 \leqslant i \leqslant j \leqslant 2), \quad [20]$$

where

$$\mathbf{E}_{11} = \begin{bmatrix} 1 & 0 \\ 0 & 0 \end{bmatrix}, \quad \mathbf{E}_{12} = \begin{bmatrix} 0 & 1 \\ 1 & 0 \end{bmatrix},$$

$$\mathbf{E}_{22} = \begin{bmatrix} 0 & 0 \\ 0 & 1 \end{bmatrix}. \quad [21]$$

Working backward from the zeroth term in this recursion yields the closed formula

$$\frac{\partial \mathbf{z}_m}{\partial v_{ij}} = \left(\sum_{l=1}^{m} \mathbf{V}^{m-l} \cdot \mathbf{E}_{ij} \cdot \mathbf{V}^{l-1}\right) \cdot \mathbf{z}_0 = \frac{\partial (\mathbf{V}^m)}{\partial v_{ij}} \cdot \mathbf{z}_0, \quad [22]$$

where $\mathbf{z}_0 = \mathbf{u}$ $(1 \leqslant i \leqslant j \leqslant 2)$. The last equality in this equation recapitulates a well-known formula for the derivative of $\mathbf{V}^m$ in the matrix direction $\mathbf{E}_{ij}$ (*11*). In practice, however, the recurrence formula in Eq. [20] is easier to use, since the derivatives of all the powers $1, \ldots, M$ are required.

The elements of the Hessian $\nabla^2\Omega$ are similarly obtained from the following recurrence relations:

$$\frac{\partial^2 \mathbf{z}_m}{\partial u_i \, \partial u_j} = \mathbf{0}, \quad \frac{\partial^2 \mathbf{z}_m}{\partial v_{ij} \partial u_k} = \mathbf{E}_{ij} \cdot \frac{\partial \mathbf{z}_{m-1}}{\partial u_k}$$

$$\frac{\partial^2 \mathbf{z}_m}{\partial v_{ij} \partial v_{kl}} = \mathbf{E}_{ij} \cdot \frac{\partial \mathbf{z}_{m-1}}{\partial v_{kl}} + \mathbf{V} \cdot \frac{\partial^2 \mathbf{z}_{m-1}}{\partial v_{ij} \partial v_{kl}} + \mathbf{E}_{kl} \cdot \frac{\partial \mathbf{z}_{m-1}}{\partial v_{ij}} \quad [23]$$

$(1 \leqslant i, k \leqslant j, l \leqslant 2)$. We note in passing that all these formulae can be extended to the case of arbitrary N-dimensional vectors $\mathbf{u}$, $\mathbf{q}_m$, and matrices $\mathbf{V}$, including nonsymmetric matrices. In addition, it is not difficult to extend them to any sequence of time points that are integer multiples of the shortest time point, just as for our linear fits.

Finally, we compute the relaxation matrix $\mathbf{R}$ from the refined estimate $\mathbf{F}_h$ of the exponential at time $t_1 = h$, exactly as described under Theory. Although this calculation can fail if the determinant $\det(\mathbf{F}_h) < \epsilon$ or the corresponding value of $|\eta\sqrt{1 + \xi^2}| > 1 - \epsilon$ in Eq. [8] for some small ϵ of order of the machine precision, this has seldom happened in any of our simulations using physically reasonable relaxation matrices and error levels; it also did not occur in our applications to experimental data (see below). Should this problem be encountered in the sorts of applications described here, the data should be checked for serious systematic errors.

In the simulations described below, as well as with the experimental data described in the next section, we have smoothed the data using a simple three-point digital filter, i.e.,

$$\bar{\mathbf{q}}_1 = (2\mathbf{q}_1 + \mathbf{q}_2)/3$$

$$\bar{\mathbf{q}}_m = (\mathbf{q}_{m-1} + 2\mathbf{q}_m + \mathbf{q}_{m+1})/4 \quad (m = 2, \ldots, M-1)$$

$$\bar{\mathbf{q}}_M = (\mathbf{q}_{M-1} + 2\mathbf{q}_M)/3. \quad [24]$$

It is also beneficial to equalize the contributions of the *a* and *b* components of the residual vector to the fit by replacing the norms in Eqs. [16] and [18] with

$$\|\tilde{\mathbf{q}}_m - \bar{\mathbf{q}}_m\|^2 \to (\tilde{a}_m - \bar{a}_m)^2(1 - w_m) + (\tilde{b}_m - \bar{b}_m)^2 w_m, \quad [25]$$

where $\tilde{\mathbf{q}}_m \equiv \mathbf{V} \cdot \mathbf{q}_{m-1}$ for Eq. [16], $\tilde{\mathbf{q}}_m \equiv \mathbf{V}^m \cdot \mathbf{u}$ for Eq. [18], and the weights are given by

$$w_m = |\bar{a}_m|/(|\bar{a}_m| + |\bar{b}_m|). \quad [26]$$

The modifications of the normal equations and derivatives required to do this are straightforward. Other choices of weights, perhaps depending on m, could shift the errors from the estimated cross-relaxation rate to the less important autorelaxation rates, but this would require a detailed knowledge of the actual error distribution in the experimental data.

RESULTS OF SIMULATIONS

The above procedures were implemented in the Matlab numerical linear algebra system, using the ''`fminu`'' routine from the optimization toolbox for the BFGS minimization. The amount of CPU required, as measured by the Matlab ''`flops`'' routine, was typically about 25,000 $\times$ M floating-point operations for each fit.

The test problems were all generated using a single relaxation matrix, which was chosen to be similar to those that were expected in the experiments we have performed (see below), namely

$$\mathbf{R} = \begin{bmatrix} -12 & -5 \\ -5 & -20 \end{bmatrix}. \quad [27]$$

A time step of approximately $h = 3\tau_{ext}/M = 0.1877/M$ was chosen, which places roughly one-third of the points before the maximum of the build-up curve, one-third between the maximum and the inflection point, and one-third after the inflection point (see Property 3 under Theory). An initial spin order $\mathbf{q}_0 = [a_0, b_0]^T$ with $a_0 = 0$ and $b_0 \in (1, 2)$ was used, and the build-up and decay curves were computed by multiplying $\mathbf{q}_0$ by the exponential $\exp(h\mathbf{R})$ a total of M times, where the number of time points M was 4, 8, or 16. The data were then generated by adding errors to the curves, according to the formula

$$\mathbf{q}_m = (\mathbf{1} + \epsilon\mathbf{r}_m)\bullet[\exp(mh\mathbf{R})\cdot\mathbf{q}_0] = \begin{bmatrix} (1 + \epsilon r_{1m})a_m \\ (1 + \epsilon r_{2m})b_m \end{bmatrix}, \quad [28]$$

where $\mathbf{r}_m = [r_{1m}, r_{2m}]^T$ is a random vector whose two components were uniformly distributed in the interval $[-1, 1]$, and the bold dot signifies element-by-element multiplication. The (relative) ''error levels'' ϵ used in our simulations were 0.1, 0.25, and 0.5.

This error model is clearly rather drastic, since the *random* errors in actual experimental data are likely to be more additive than multiplicative, and their distribution, even if not Gaussian, will at least tend to fall off with increasing size. Measurements of cross-peak intensities, however, are often afflicted by outliers and systematic deviations, whose expected magnitudes can at best be bounded from above. Without knowing how these sorts of errors are distributed, it is pointless to attempt to determine the resulting probability distribution in the results. The above error model does at least enable us to obtain worst-case bounds on the magnitude of the relative errors that can be expected in the results, given the bounds on the relative errors ϵ in the data. This is the standard method of quantifying the sensitivity of a function to perturbations.

For each of the nine possible combinations of these three values each of M and ϵ, we generated a total of 100 test problems and ran our fitting procedures on each. The *relative error matrix* was calculated from the resulting relaxation matrices as

$$\begin{bmatrix} (\rho_x^{calc} - \rho_x)/\rho_x & (\sigma^{calc} - \sigma)/\sigma \\ (\sigma^{calc} - \sigma)/\sigma & (\rho_y^{calc} - \rho_y)/\rho_y \end{bmatrix}, \quad [29]$$

and the minimum, maximum, and RMS (root-mean-square) values for each of the three independent entries in this matrix were computed over all the runs which converged. The results obtained by fitting the weighted and smoothed data are summarized in Table 1.

It will be observed that, providing eight or more time points were used, the relative errors in the cross-relaxation rate σ were comparable to the relative errors in the measurements, on the average. It will also be observed that the errors in the auto-relaxation rate ρ_a were considerably larger than the errors in σ, whereas the errors in the other auto-relaxation rate ρ_b were considerably smaller. This is consistent with the fact that the initial condition had $a_0 = 0$, so that all knowledge of ρ_a was derived from the relatively weak build-up curve. Finally, it can be seen from the differences in the minimum and maximum relative errors that some of the estimates, most notably those obtained from only four time points, were extremely biased. In particular, ρ_a and σ were systematically too high, whereas ρ_b was systematically too low.

By further refining the values obtained from fitting the smoothed data against the unsmoothed data (Table 2), these biases were found to be primarily due to the smoothing procedure. The RMS relative errors in the rates also tended to be less when fitting the unsmoothed data. In this regard, it should further be observed that the fits of the calculated curves to the smoothed data (''calcd to data'' in Table 1) were generally better than the corresponding fits to the unsmoothed data (''calcd to data'' in Table 2); i.e., the smoothed data can generally be fit more closely than the unsmoothed. The fits of the calculated curves to the curves obtained from the exact relaxation matrix in Eq. [27] (''calcd to exact'' in Table 1) were generally nevertheless *worse* than the corresponding fits to the smoothed data (''calcd to data'' in Table 1), whereas the opposite was observed with the fits to the unsmoothed data (Table 2). These observations are another symptom of the bias introduced by smoothing. For comparison, the fits of the data to the exact curves (''data to exact'' in the tables) are also given.

Unfortunately, the fits to the unsmoothed data were also numerically more difficult to compute, and Newton's method more frequently diverged when the number of time points was small and the error level high. Direct fitting of the unsmoothed data, without first fitting the smoothed data, diverged even more often. Fortunately, by first fitting the smoothed data, the convergence rate obtained with reasonably good unsmoothed data at eight or more time points remained acceptable. Therefore, until a less biased smoothing strategy can be developed, this final optimization against the unsmoothed data is strongly recommended. Figure 1 shows plots of the perturbed data, the smoothed data, the final fit to the unsmoothed data, and the exact solution, for a typical problem with eight time points and a 25% error level.

In summary, our simulations indicate that whenever data at eight or more time points are available and the true 2×2 relaxation matrix is similar to that shown in Eq. [27], our method of fitting the build-up and decay curves will usually

TABLE 1
Results of Simulated Test Problems (Smoothed)[a]

Time points:	4			8			16		
Error level:	10%	25%	50%	10%	25%	50%	10%	25%	50%
Weighted sum of squares									
Mean ($\times 10^{-3}$)									
Calcd to data	1.67	2.46	5.38	3.68	8.35	24.1	4.39	10.5	25.8
Calcd to exact	6.96	16.1	49.2	3.90	11.7	45.7	2.99	10.3	31.6
Data to exact	8.66	18.5	55.1	7.67	20.3	70.8	7.47	21.2	57.7
ρ_a in-phase decay rates									
% Error									
RMS	65.0	109.4	174.5	14.3	24.5	62.0	7.8	16.9	34.6
Minimum	4.2	−63.9	−184.3	−12.5	−41.7	−99.0	−3.2	−18.7	−36.8
Maximum	123.4	313.3	948.4	36.6	70.2	198.0	17.6	45.6	122.5
ρ_b antiphase decay rates									
% Error									
RMS	18.9	20.6	31.8	6.7	9.5	14.6	4.6	6.1	8.4
Minimum	−30.1	−47.3	−87.1	−12.0	−20.9	−32.3	−8.7	−14.8	−20.3
Maximum	0.0	13.3	51.9	0.0	14.1	34.3	1.2	5.9	19.5
σ cross-relation rates									
% Error									
RMS	29.5	49.1	82.8	11.4	19.2	45.7	7.5	18.0	35.8
Minimum	0.2	−32.2	−60.9	−9.8	−21.4	−55.1	−8.2	−18.4	−38.5
Maximum	65.7	154.3	413.0	31.3	59.3	171.1	18.8	53.5	126.8
Optimizer convergence rate									
% Success									
Out of 100	100	100	92	100	100	98	100	100	99

[a] The first row, labeled ''Time points,'' contains the numbers of time points M that were used. The second, labeled ''Error level,'' contains the values of ϵ that were used to perturb the simulated data, as in Eq. [28]. The first set of rows, labeled ''Weighted sum of squares,'' contains the values of the fits, weighted in accord with Eq. [26], between the perturbed smoothed data (data), the exact solution simulated from the relaxation matrix in Eq. [27] (exact), and the solution calculated from the fitted rates and initial spin orders (calcd). The following three sets of rows contain the root-mean-square average of the relative errors in each of the rates ρ_x, ρ_y, and σ, computed according to Eq. [29] (RMS), along with the minimum and maximum relative errors over all converging runs. The last row of the table contains the number of runs which converged out of the total 100 random perturbations.

produce rates whose relative errors are less than the largest relative errors in the data. This shows that the problem of estimating the rates, as formulated in this paper, is not ill conditioned. There is, of course, always a chance that all of the errors in the data are either positive or negative, and in this case a strong deviation of the estimated rates from the exact rates is simply inevitable. This is, in fact, the reason for the very large minimum and maximum errors that were obtained with only four time points. Although a substantial amount of spectrometer time is required to collect data at eight time points, it reduces the probability of such strong deviations to only 1/128 (assuming unbiased errors). Therefore the experiments that we shall now describe used data collected at eight time points.

RESULTS WITH EXPERIMENTAL DATA

Cross correlation between the $^{15}N-{}^{1}H$ dipole–dipole interaction and the chemical-shift anisotropy (CSA) of the nitrogen in the amide groups of proteins induces interconversion of the in-phase and antiphase nitrogen spin orders. The rate for this process is given by (*2, 6, 13, 14*)

$$R_{IN}(N_x \leftrightarrow 2I_zN_x) = K[\tfrac{2}{3}J(0) + \tfrac{1}{2}J(\omega_N)], \qquad [30]$$

where $K = (\hbar\gamma_I\gamma_N\omega_N\Delta_N\langle P_2(\cos\varphi)\rangle)/r_{IN}^3$ depends both on the magnitude of the CSA Δ_N and on the second Legendre polynomial P_2 of the cosine of the angle φ between the

TABLE 2
Results of Stimulated Test Problems (Unsmoothed)[a]

Time points:	4			8			16		
Error level:	10%	25%	50%	10%	25%	50%	10%	25%	50%
				Weighted sum of squares					
Mean ($\times 10^{-3}$)									
Calcd to data	2.22	9.06	45.2	3.24	22.2	85.4	3.77	25.5	94.3
Calcd to exact	2.01	12.7	51.6	1.62	10.3	45.6	1.51	9.58	34.5
Data to exact	4.22	21.8	97.9	4.86	32.5	131.	5.28	35.2	128.
				ρ_a in-phase decay rates					
% Error									
RMS	24.6	70.1	172.4	9.6	20.8	54.7	4.5	13.4	29.2
Minimum	−56.1	−121.6	−286.0	−20.1	−46.4	−105.3	−9.5	−22.8	−42.9
Maximum	57.7	216.0	768.1	26.5	58.1	158.4	8.9	38.6	105.4
				ρ_b anti-phase decay rates					
% Error									
RMS	8.2	17.7	35.9	3.1	8.8	16.3	2.4	6.5	11.7
Minimum	−17.1	−39.5	−81.7	−6.6	−17.9	−35.4	−5.0	−13.0	−18.5
Maximum	18.1	43.2	60.0	6.4	25.0	50.0	6.2	14.8	37.1
				σ cross-relaxation rates					
% Error									
RMS	11.0	30.2	74.6	7.1	15.7	39.6	5.2	15.3	31.8
Minimum	−22.4	−51.0	−52.0	−14.7	−25.0	−59.9	−13.7	−21.0	−41.0
Maximum	32.9	106.9	327.5	21.2	48.1	149.8	11.7	47.1	105.8
				Optimizer convergence rate					
% Success									
Out of 100	100	96	56	100	100	98	100	100	96

[a] The labels in this table have the same meaning as in Table 1, except that the data used here were not smoothed.

principal axis of the chemical-shift tensor and the $^{15}N-{}^{1}H$ bond vector.

These rates provide further constraints for use in the spectral-density mapping procedure developed by Peng and Wagner (*15*) (which is currently capable of determining the value of the spectral density at only two frequencies), and contain additional conformational and dynamic information by virtue of their dependence on the angle φ (*16*). Although experiments have recently been proposed which yield data that depend on these rates (*16, 17*), a general method of estimating the rates from these data and assigning error bars to the estimates has not. Therefore, such experiments provide an excellent demonstration for the method we have developed in this paper.

As our sample, we used a 3 m*M* solution of uniformly ^{15}N-enriched oxidized flavodoxin from *A. nidulans* at pH 6.6 and 303 K. This 169-residue protein yields excellent spectra for its size, and has been the subject of a thorough relaxation analysis using the Lipari–Szabo and reduced-spectral-density formalisms (*18*). The decay of antiphase coherence was measured as described in (*15*). The pulse sequence used to measure the conversion of antiphase to in-phase coherence is a modification of the spin-locked antiphase experiment proposed earlier (*5, 7, 15*), with the omission of the 180° proton pulses during the relaxation period. Instead of decoupling during acquisition, the two components of each doublet were integrated separately and their intensities added together to average over both noise and artifacts. It should be understood that these experiments are still under development, and at this time the numbers we have derived from them should be regarded as preliminary.

Both the spectra designed to measure antiphase decay as well as in-phase build-up were collected at eight time points equally spaced at intervals of 32 ms. Since the pulse sequences used to measure the in-phase and antiphase coherence differed in length by only about 6 ms, the cross-peak

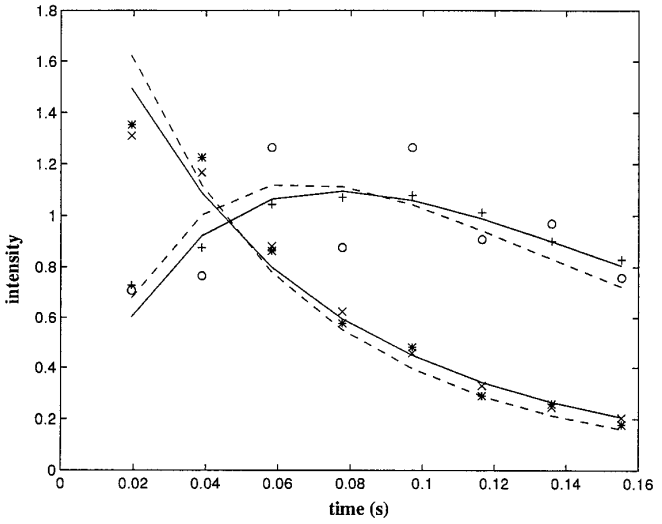

FIG. 1. Plots of perturbed negative build-up (circles) and decay (asterisks) data, the corresponding smoothed data (pluses and crosses), the final fit to the unsmoothed data (solid lines), and the exact solution (dashed lines), for a simulated problem using eight time points and a 25% error level. The build-up data and curves have been scaled by a factor of four for easier viewing.

intensities measured in the two experiments should be on very nearly the same scale. After trying several different peak-integration procedures, we concluded that none worked significantly better than simply measuring the height of each cross peak. The heights of both the in-phase and the antiphase cross peaks were normalized by dividing them by the height of the antiphase cross peak at the first time point. Thus the data set $\mathbf{q}_m = [a_m, b_m]^{\mathrm{T}}$ $(1 \leqslant m \leqslant 8)$ for each amide group consisted of two sequences of eight normalized cross-peak heights, where $a \equiv \langle N_x \rangle$ and $b \equiv \langle 2I_z N_x \rangle$. Twenty-four of the 165 potential pairs of cross peaks (169 residues − 3 prolines − 1 N-terminus) could not be measured because they were either too weak or overlapped with other cross peaks; these have simply been omitted from the following discussion and figures.

In addition to simply applying our procedure to each of these 141 data sets, we also performed a Monte Carlo analysis in order to establish error bars on the estimated rates. This was done by computing the (unweighted) sum of the squares of the deviations between the fitted curves and the (unsmoothed) data, dividing by the number, 16, of data points, and using the square root of the result as the standard deviation for 200 independent perturbations of the data by the addition of Gaussian random numbers. Our procedure was run on each of these 200 perturbed data sets, and the RMS deviation from the rates estimated from the unperturbed data was taken as an estimate of the standard deviation in the rates. Therefore, unlike our simulated test problems, the errors we report here should be regarded as conservative estimates of the true errors, which make no allowance for outliers or systematic deviations.

A visual presentation of the results is given in Figs. 2 through 4; a complete table containing all the numerical values is available from the authors. The following statistics will be useful in discussing these results:

1. The average of the estimated rates along the sequence, which is obtained simply by adding up the rates over all amino acids at which estimates were successfully obtained, and dividing by the number of such amino acids.
2. The average of the standard deviations in the rates along the sequence, where these standard deviations were estimated from the Monte Carlo procedure described above.
3. The standard deviation in the estimated rates from their average along the sequence, as defined in 1 (above); note that this has no direct connection to the average standard deviation defined in 2!

All rates are given in units of inverse seconds.

The average of the estimated in-phase decay rates along the sequence was 8.71, while their average estimated standard deviations was 0.83. Most of the larger deviations from the average are associated with large estimated standard deviations (Fig. 2), and hence are not statistically significant. While some systematic variations in the rates along the sequence can be seen, they are at most twice the average estimated standard deviation, and the standard deviation of the estimated rates from their average along the sequence is only 1.03. This lack of large sequence variations in the rates is consistent with that observed in independent measure-

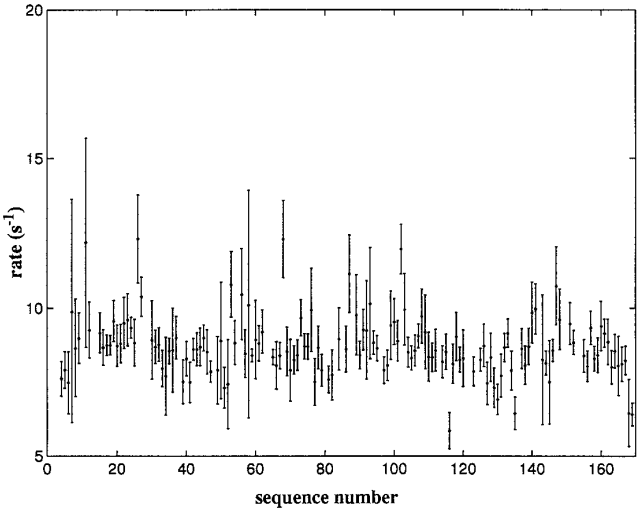

FIG. 2. Plots of the in-phase decay rates versus amino acid sequence number, in units of inverse seconds. The estimated value of the rate is located at the center of each vertical line in the plot, and the length of each line is equal to twice the estimated standard deviation in its value (see text).

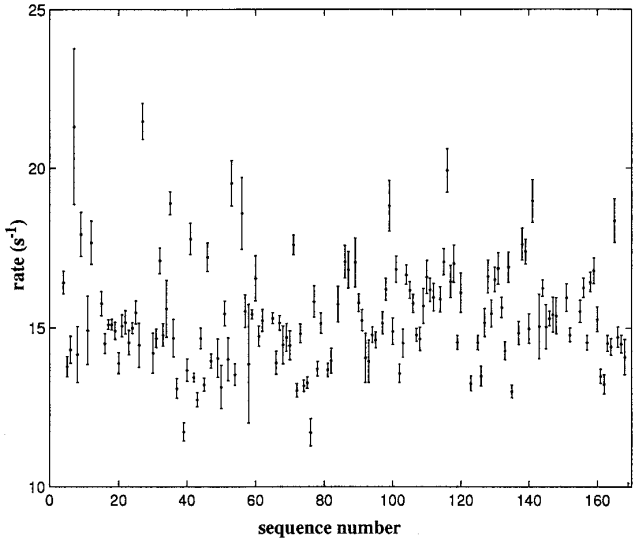

FIG. 3. Plots of antiphase decay rates versus amino acid sequence number. The units and symbols in this plot have the same meanings as in Fig. 2.

ments of $T_{1\rho}^{-1}$ (*18*), and it is therefore not surprising that the RMS difference between our rates and the $T_{1\rho}^{-1}$ rates (over the 133 amino acids at which both were available) is only 1.00. The average of the $T_{1\rho}^{-1}$ rates along the sequence is 9.16, however, which indicates that these latter rates tend to be slightly larger than ours.

As was expected from our simulations, our estimated antiphase decay rates are substantially more precise, with standard deviations of only 0.44 on the average. It is interesting to observe that there is considerably more scatter in the antiphase rates than in the in-phase rates, with a standard deviation from the average of 1.73 (Fig. 3). This is consistent with the fact that the antiphase decay rates include contributions from proton–proton dipole–dipole interactions, which vary with the density of neighboring protons along the sequence. In this case, the RMS difference with the 133 antiphase decay rates that were also determined independently by monoexponential fits with suppression of cross correlation (*18*) was 2.61. Much of this difference was due to the difference in the average rates along the sequence, which were 15.32 and 17.25 for the rates determined here and those determined with suppression of cross correlation, respectively.

The cross-relaxation rates σ again appear to be reasonably well determined by the data, with estimated values and standard deviations averaging 5.63 and 0.35 along the sequence, respectively (Fig. 4). The standard deviation along the sequence is 0.99. As before, the larger deviations from the average tend to be associated with larger estimated standard deviations, but not always. One such case occurs at Asn-135, which yielded the unusually low cross-relaxation rate of 3.00 ± 0.13; this amino acid is located in a highly acid and nonconserved loop. The only comparably small cross-relaxation rates occurred on the epsilon-nitrogen of Trp-66 (not shown). Unusually large rates exceeding 8 were observed in several places, the most convincing of which were found in another loop at both Gly-26 and Gly-27 (8.08 and 9.66, respectively). The largest single antiphase decay rate was also observed at Gly-27 (21.49), and there was a significant overall correlation between the antiphase decay rates and the cross-relaxation rates, with a correlation coefficient of 0.63. The correlation between the in-phase decay rates and the cross-relaxation rates was 0.35, while the in-phase and antiphase rates were essentially uncorrelated at 0.10.

We conclude that, although many of the differences and trends that may be seen in Figs. 2 through 4 are certainly real and contain structural and dynamic information, improved experiments will be needed in order to obtain the rates with higher precision before their full significance can be assessed. Such experiments are currently under development in our laboratory.

CONCLUSIONS

We have described a novel procedure for estimating small relaxation matrices, and we have shown that it gives good results on typical 2 × 2 problems. In contrast, this laboratory's experience has been that a ''naive'' implementation of an approach based on multiexponential fits (as described in the Introduction) is extremely sensitive to errors in simulated data, and even to the convergence criterion used to compute the multiexponential fit. More reasonable results can be ob-

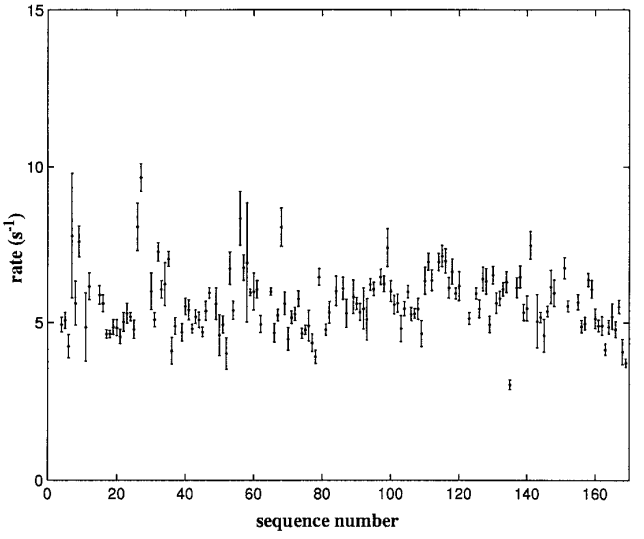

FIG. 4. Plots of in-phase to antiphase cross-relaxation rates versus amino acid sequence number. The units and symbols in this plot have the same meanings as in Fig. 2.

tained through a determined effort to stabilize these fits, for example, by appropriate smoothing and weighting procedures, or by regularization functional methods. Comparing our method with all possible variants of methods based on multiexponential fits is outside the scope of this paper, but the sensitivity of multiexponential fits to errors in the data is well known to researchers in many different fields of science and engineering. It is therefore quite certain that better results will generally be obtained with less effort from an approach that fits the exponential of the relaxation matrix directly as we have done here. This approach is also less labor intensive than the multiple experiments that are needed to determine the rates one at a time from scalar (multi) exponential fits.

Although we have illustrated the approach here for the special case of cross correlation-induced cross relaxation between the in-phase and antiphase nitrogen coherence of the amide groups of proteins, the method should be readily generalized to a wide variety of other molecular relaxation processes. The method can also be extended, in a straightforward fashion, to the estimation of larger relaxation matrices containing many more independent rates, providing that measurements at a sufficiently large number of time points are available. Alternatively, one could collect data for multiple initial conditions, as illustrated, for example, in (*19*).

In particular, symmetric two-dimensional spectra such as NOESY in principle contain the results of experiments performed for all possible initial conditions of the form [1, 0, . . . , 0], [0, 1, . . . , 0], . . . , [0, 0, . . . , 1] (i.e., with all coherence initially in one spin order). In practice, the presence of numerous missing and/or overlapping cross peaks would greatly complicate the application of methods like that described in this paper, which would also become computationally extremely demanding. Nevertheless, we believe that such an approach could yield better results (and is at least more direct) than the numerous ''bootstrap'' methods that have been developed for estimating large relaxation matrices from NOESY spectra [see, e.g., (*20*)], particularly if used in conjunction with the spectrum decomposition methods introduced in Ref. (*21*). Further work along these lines is in progress.

ACKNOWLEDGMENTS

This work was supported by NIH Grants GM-47467 and GM-38221 and NSF Grant DBI-951185.

REFERENCES

1. L. G. Werbelow, *in* ''Understanding Chemical Reactivity'' (R. Tycko, Ed.), Vol. 8, p. 223–263, Kluwer, Dordrecht/Boston/London, 1994.
2. J. W. Peng and G. Wagner, *in* ''Understanding Chemical Reactivity'' (R. Tycko, Ed.), Vol. 8, p. 373–454, Kluwer, Dordrecht/Boston/London, 1994.
3. A. Kumar and P. K. Madhu, *Concepts Magn. Reson.* **8,** 139–160 (1996).
4. J. Boyd, U. Hommel, and I. D. Campbell, *Chem. Phys. Lett.* **175,** 477–481 (1990).
5. A. G. Palmer III, N. J. Skelton, W. J. Chazin, P. E. Wright, and M. Rance, *Mol. Phys.* **75,** 699–712 (1992).
6. M. Goldman, *J. Magn. Reson.* **60,** 437–452 (1984).
7. L. E. Kay, L. K. Nicholson, F. Delaglio, A. Bax, and D. A. Torchia, *J. Magn. Reson.* **97,** 359–375 (1992).
8. H. R. Halvorson, *in* ''Methods in Enzymology'' (L. Brand and M. L. Johnson, Eds.), Vol. 210, p. 54–67, Academic Press, San Diego, 1992.
9. P. J. Rousseeuw and A. M. Leroy, ''Robust Regression & Outlier Detection,'' Wiley, New York, 1987.
10. J.-X. Yang and T. F. Havel, *J. Biomol. NMR* **3,** 355–360 (1993).
11. I. Najfeld and T. F. Havel, *Adv. Appl. Math.* **16,** 321–375 (1995).
12. F. R. Gantmacher, ''The Theory of Matrices,'' Vol. 2, Chelsea, Bronx, New York, 1959.
13. S. Wimperis and G. Bodenhausen, *Mol. Phys.* **66,** 897–919 (1989).
14. R. Brüschweiler and R. R. Ernst, *J. Chem. Phys.* **96,** 1758–1766 (1992).
15. J. W. Peng and G. Wagner, *J. Magn. Reson.* **98,** 308–332 (1992).
16. K. T. Dayie, P. Zhang, and G. Wagner, Experimental NMR Conference, Poster MP57, Asilomar, 1994.
17. J. R. Tolman and J. H. Prestegard, *J. Magn. Reson. B* **106,** 97–100 (1995).
18. P. Zhang, K. Dayie, and G. Wagner, *J. Mol. Biol.,* in press.
19. B. T. Bulliman, P. W. Kuchel, and B. E. Chapman, *J. Magn. Reson.* **82,** 131–138 (1989).
20. H. Liu, H. P. Spielmann, N. B. Ulyanov, D. E. Wemmer, and T. L. James, *J. Biomol. NMR* **6,** 390–402, 1995.
21. T. F. Havel, I. Najfeld, and J.-X. Yang, *Proc. Natl. Acad. Sci. USA* **91,** 7962–7966 (1994).